

## Influence of bainite reaction on the kinetics of carbon redistribution during the Quenching and Partitioning process

Nishikawa, Arthur S.; Santofimia Navarro, Maria; Sietsma, Jilt; Goldenstein, Hélio

**DOI**

[10.1016/j.actamat.2017.09.048](https://doi.org/10.1016/j.actamat.2017.09.048)

**Publication date**

2018

**Document Version**

Accepted author manuscript

**Published in**

Acta Materialia

**Citation (APA)**

Nishikawa, A. S., Santofimia Navarro, M., Sietsma, J., & Goldenstein, H. (2018). Influence of bainite reaction on the kinetics of carbon redistribution during the Quenching and Partitioning process. *Acta Materialia*, 142, 142-151. <https://doi.org/10.1016/j.actamat.2017.09.048>

**Important note**

To cite this publication, please use the final published version (if applicable). Please check the document version above.

**Copyright**

Other than for strictly personal use, it is not permitted to download, forward or distribute the text or part of it, without the consent of the author(s) and/or copyright holder(s), unless the work is under an open content license such as Creative Commons.

**Takedown policy**

Please contact us and provide details if you believe this document breaches copyrights. We will remove access to the work immediately and investigate your claim.

# Influence of bainite reaction on the kinetics of carbon redistribution during the Quenching and Partitioning process

Arthur S. Nishikawa<sup>a,\*</sup>, Maria J. Santofimia<sup>b</sup>, Jilt Sietsma<sup>b</sup>, H elio Goldenstein<sup>a</sup>

<sup>a</sup>Department of Metallurgical and Materials Engineering, University of S ao Paulo, Av. Prof. Mello Moraes, 2463, 05508-030, S ao Paulo, Brazil

<sup>b</sup>Department of Materials Science and Engineering, Delft University of Technology, Mekelweg 2, Delft, 2628 CD, The Netherlands

## Abstract

In the present study the microstructural evolution and kinetics of carbon redistribution during the partitioning step of the Quenching and Partitioning process are investigated by means of a modeling approach that simultaneously considers the martensite-austenite carbon partitioning and the decomposition of austenite into bainitic ferrite. The development of the phase fractions, interface position, and carbon compositions are analyzed for two different binary Fe-C alloys with distinct initial carbon compositions and simulation geometries. The composition dependence of carbon diffusivity in austenite is taken into account for solving the diffusion field equations. Simulations indicate that kinetics of carbon partitioning from martensite to austenite is controlled by carbon diffusion in martensite and it is little affected by simultaneous occurrence of bainite reaction. On the other hand martensite-austenite carbon partitioning strongly influences the bainite reaction by inhibiting the growth of bainitic ferrite.

**Keywords:** Quenching and Partitioning; Bainite; Modeling; Mixed-mode model

## 1. Introduction

The Quenching and Partitioning (Q&P) process was proposed by Speer and coworkers in 2003 [1] as a new heat treatment route to obtain bcc + fcc multiphase microstructures with optimum properties [1, 2]. The Q&P process involves quenching of austenite between the martensite-start (Ms) and room temperatures to produce a controlled mixture of martensite ( $\alpha'$ ) + austenite ( $\gamma$ ). Then, in the so called "partitioning" step, the material is isothermally held at a higher temperature to promote the diffusion of the carbon in the supersaturated martensite to the untransformed austenite. Thus the partitioning step is intended to carbon-enrich the austenite, allowing its stabilization at room temperature. The success of this process depends on the suppression of competitive reactions that act as sinks for carbon, particularly carbides precipitation. Cementite suppression can be achieved by controlled additions of alloying elements that delay its formation, e.g. silicon and aluminum. In the resulting Q&P microstructure martensite confers high strength, whereas stabilized austenite favors good ductility due to occurrence of TRIP effect [3].

The essential mechanism of the Q&P process is the carbon redistribution from martensite to austenite. Speer et al. [1] have proposed that the endpoint of carbon partitioning can be modeled assuming a "constrained carbon equilibrium" (CCE). The CCE hypothesis assumes that during the partitioning step the mobility of iron and the substitutional species can be neglected, competitive reactions (e.g., carbides precipitation, decomposition of austenite) are fully suppressed, and the martensite-austenite interface can be assumed immobile or stationary. The

*constrained equilibrium* is therefore reached by equilibration of carbon's chemical potential only ( $\mu_C^{\alpha'} = \mu_C^{\gamma}$ ). Initially, an infinite set of compositions in martensite and austenite can fulfill this relation. However, once this condition is coupled with the conservation equations derived from the other assumptions, a given composition of austenite leads to a unique corresponding composition in martensite.

Currently, theoretical considerations and experimental observations question the assumptions of the CCE model. Migration of martensite-austenite interface has been directly observed by in-situ transmission electron microscopy [4] and its relevance discussed by computational models [5, 6]. Besides, competitive reactions are not always avoided during the Q&P process, even in carefully designed alloys. It has been reported that transition carbides can tolerate much more Si than cementite and might form in different stages of the heat treatment, despite high alloying addition [7, 8]. Yet, formation of fine transition carbides by martensite tempering is usually not considered detrimental, whereas cementite can be of more concern [9]. Decomposition of austenite may also take place during Q&P. The normally employed range of partitioning temperatures enables the bainite formation from austenite. Nevertheless, because of high silicon content, bainite formation in Q&P steels is reported to happen with absence of carbides (i.e., only bainitic ferrite) [10, 7]. Thus, similarly to TRIP-assisted steels, bainite reaction in Q&P steels contributes to carbon enrichment of the surrounding austenite. However, decomposition of austenite decreases the fraction of austenite in the final product, affecting the properties of the final product. Modern Q&P alloys have been designed with higher manganese and nickel content to improve the hardenability of the austenite, decreasing the kinetics of bainite formation [2, 11]. However, employment of large fractions

\*Corresponding author. Email: arthur.nishikawa@usp.br

of alloying elements increases the production costs and may imply processing difficulties due to, for example, development of segregation bands. This is even more critical when considering the Q&P applied to cast products, such as cast iron, where the microsegregation formed during solidification is not mitigated by further thermomechanical processing [12].

It is clear that a better view of how the competitive reactions affect the microstructural evolution during the Q&P process is necessary, as it strongly influences the final properties of the material. A physically-based model that accounts for the involved metallurgical processes can provide a fundamental understanding of how the interactions between the different phenomena affect the final microstructure.

Different models are available in the literature for describing the carbon partitioning from a supersaturated bcc phase to an fcc phase, either considering interface migration or not. The problem was first addressed by Mujahid and Bhadeshia [13] and by Hillert et al. [14] in the context of the discussion of the mechanism of bainite reaction. In both papers the authors performed one-dimensional (1D) simulations to solve Fick's second law for the bulk phases and evaluated the kinetics of decarburization of a carbon-supersaturated ferrite plate. As boundary conditions, Mujahid and Bhadeshia assumed fixed compositions determined by paraequilibrium at the  $\alpha'/\gamma$  interface. Hillert argued that this assumption would lead to a discontinuity in the chemical potential of carbon at the interface. Alternatively, they proposed a condition of "local equilibrium for carbon" at the interface, in which the equality of chemical potentials is obeyed, albeit only for the carbon. This hypothesis is essentially the same used by Speer et al. [1] in the formulation of the CCE theory. Most recently, the carbon partitioning under the influence of a mobile  $\alpha'/\gamma$  interface has been approached by calculating the diffusion fields of carbon in a 1D grid [5, 6] and by phase-field modeling in two and three dimensions [15, 16]. These studies have relied on Hillert's local equilibrium for carbon as thermodynamical condition at the interfaces.

The local kinetics of diffusional growth of ferrite from austenite at high temperatures has been extensively reported in the literature. However, modeling the formation of Widmanstätten/bainitic ferrite is particularly challenging, given that there is still no agreement about the mechanism of its growth. The two concurrent schools dispute whether the bainite reaction takes place with or without diffusion during the growth of subunits, implying different thermodynamical conditions for its growth [17, 18]. According to the diffusionless theory, bainitic ferrite grows by successive nucleation and growth of subunits by a displacive mechanism until the carbon content in austenite reaches the  $T_0$  limit. When  $T_0$  is reached, the free energies of fcc and bcc are equal and, consequently, there should be no driving force for nucleation of new bainite subunits. Conversely, the diffusional theory states that bainite grows by a reconstructive mechanism controlled by diffusion of carbon [19, 20, 21]. The thermodynamical limit for the transformation in these conditions is assumed to be the meta-stable equilibrium between ferrite and austenite. In turn, since mobilities of substitutional elements at the range of temperatures for bainite formation are very low, paraequilibrium condition is normally invoked to de-

scribe this limit.

None of the proposed mechanisms for bainite reaction seems to describe the experimental results perfectly well. Experimental points often lie beyond the  $T_0$  line for low temperatures and below it for high temperatures [22]. Similarly, the paraequilibrium lines also fails to accurately describe the thermodynamical limit for bainite reaction. Efforts have been made on both sides of the dispute to obtain a better description of the phenomenon. Among the researchers that defend the diffusional view it is of general agreement that the transformation stasis is caused by dissipation of the chemical driving force by solute drag at the interfaces [23]. A few studies have achieved some success in predicting the bainite stasis using a so called GEB (Gibbs energy balance) theory concurrently with an analytical solution of the mixed-mode model [24, 25]. However, it is reported that even in similar conditions of temperature and composition the solute drag theory can encounter problems for supporting the experimental data [26].

An alternative theory for describing the thermodynamical limits of the bainite reaction was proposed by Hillert and coworkers [22]. Hillert postulated the existence of a thermodynamical barrier for the growth of bainitic ferrite. Using experimental data, the authors determined that the additional energies for bainite formation at 700, 450, and 300 °C are 107, 1283, and 2329 J/mol, respectively. These values were then interpolated using a spline to get a smooth curve describing the variation of the extra energy with the temperature. Using the modified free energies of ferrite it was possible to obtain the thermodynamical limit for the growth of Widmanstätten and bainitic ferrite, a so called *WBs* limit. The *WBs* theory was able to predict reasonably well the phase fractions and the austenite carbon content for several alloys, even when the effects of different alloying elements were considered.

In the present study the microstructural evolution and kinetics of carbon redistribution during the partitioning step of the Q&P process are investigated by means of a modeling approach that simultaneously considers the martensite-austenite carbon partitioning and the decomposition of austenite into bainitic ferrite (henceforth, *coupled model*). The evolution of the phase fractions, interface position, and carbon compositions are analyzed for two different binary Fe-C alloys with distinct initial carbon compositions and simulation geometries. A more accurate assumption which considers the composition dependence of carbon diffusivity in austenite is taken into account for solving the diffusion field and the results are compared to the generally adopted constant diffusivity approach.

## 2. Model

The kinetic model for carbon diffusion has been implemented by numerically solving the laws of diffusion by means of a 1D finite-difference method (FDM). For modeling purposes, it is assumed that martensite has a bcc structure supersaturated in carbon. The main assumptions of the CCE theory are considered for modeling the carbon diffusion from martensite to austenite. Thus, during the partitioning step, the carbon in martensite is redistributed to austenite without movement of the inter-

face and with no partitioning of substitutional elements. At the  
 175 martensite-austenite interface the chemical potentials of carbon  
 in both phases are set equal (local equilibrium for carbon). This  
 is a necessary assumption in order to guarantee the continuity of  
 the chemical potential along the interface. These assumptions  
 imply that for a given composition of austenite at the interface  
 180 there is a unique corresponding composition in martensite.

The growth of bainitic ferrite ( $\alpha_b$ ) from the austenite has  
 been modeled using a mixed-mode approach for describing the<sup>220</sup>  
 sidewise movement of the ferrite-austenite interfaces (plate-thick-  
 ening). Only the plate-thickening kinetics has been considered  
 185 because both the thickening and lengthening cannot be simul-  
 taneously represented in the 1D case. The plate-thickening sce-  
 nario represents the growth of a bainitic ferrite lath oriented in<sup>225</sup>  
 parallel to the martensite plate. In turn, the foundation of the  
 mixed-mode model is based on an energy balance between the  
 190 available chemical driving force for movement of the interface  
 ( $\Delta G^{chem}$ ) and the dissipated energy due to the interface migra-  
 tion ( $\Delta G^{fric}$ ). These two terms can be expressed as follows:

$$\Delta G^{chem} = \sum_i x_i^\alpha (\mu_i^\gamma - \mu_i^\alpha) \quad (1)$$

$$\Delta G^{fric} = V_m \frac{v}{M} \quad (2)$$

where  $x_i^\alpha$  is the concentration of the component  $i$  in the grow-  
 ing phase  $\alpha$ ,  $\mu_i^p$  is the chemical potential of  $i$  in the phase  $p$ ,  
 195  $V_m$  is the molar volume of the growing phase,  $M$  the interface  
 mobility, and  $v$  the interface velocity, which assumes positive  
 values for the ferrite growth. At the interface the local equi-  
 librium of carbon is assumed, so that  $\Delta G^{chem}$  arises from the<sup>230</sup>  
 differences of chemical potentials of iron and the substitutional  
 200 species, while  $\Delta G^{fric}$  is function of the interface velocity and  
 the interface mobility. By equating these two terms an expres-  
 sion for the interface velocity in Fe-C system is obtained, as  
 follows:

$$v = \frac{M}{V_m} x_{Fe}^\alpha (\mu_{Fe}^\gamma - \mu_{Fe}^\alpha) \quad (3)$$

The interface mobility  $M$  is expressed in the familiar Arrhe-<sup>235</sup>  
 nius form,  $M = M_0 \exp[-Q_a/(RT)]$ . In this work the param-  
 205 eters suggested by Gamsjäger et al. [27, 28],  $M_0 = 2 \times 10^{-4} \text{ m}^4 \text{ J}^{-1} \text{ s}^{-1}$   
 and  $Q_a = 140\,000 \text{ J mol}^{-1}$ , were used.

The diffusion of carbon in martensite, austenite, and during  
 the growth of bainitic ferrite is modeled by numerically solving<sup>240</sup>  
 Fick's second law of diffusion. The numerical solution for in-  
 210 creasing partitioning times is determined by a finite-difference  
 method (FDM) assuming that the diffusion coefficient of car-  
 bon in austenite varies as a function of the composition. This  
 assumption is more physically accurate than the traditional con-  
 stant diffusivity approach, as the carbon diffusivity in austenite  
 215 is strongly sensitive to the carbon content [14]. Fick's second<sup>245</sup>  
 law was discretized implicitly for the derivatives of the compo-  
 sition and explicitly for the gradient of the diffusion coefficient  
 following the equations:

$$c_i^t = -(r_i + g_i) c_{i+1}^{t+1} + (1 + 2r_i) c_i^{t+1} - (r_i - g_i) c_{i-1}^{t+1} \quad (4)$$

$$r_i = D_i \frac{\Delta t}{\Delta z^2} \quad (5)$$

$$g_i = \frac{D_{i+1} - D_{i-1}}{4} \frac{\Delta t}{\Delta z^2} \quad (6)$$

where the indices  $i$  and  $t$  refer respectively to the node posi-  
 tion and the time step,  $c_i^t$  is the mole fraction of carbon,  $D_i$   
 is the diffusion coefficient of carbon,  $\Delta t$  is the time step and  $\Delta z$   
 is the step size. The diffusion coefficients of carbon in austenite  
 and ferrite/martensite phases were calculated using the equa-  
 tions determined by Ågren [29, 30]:

$$D_C^\gamma = 4.53 \times 10^{-7} \left[ 1 + y_C^\gamma (1 - y_C^\gamma) \frac{8339.9}{T} \right] \\ \times \exp \left[ - \left( \frac{1}{T} - 2.221 \times 10^{-4} \right) (17767 - 26436 y_C^\gamma) \right] \quad (7)$$

$$D_C^\alpha = 2 \times 10^{-6} \exp \left( - \frac{10115}{T} \right) \\ \times \exp \left\{ 0.5898 \left[ 1 + \frac{2}{\pi} \arctan \left( 1.4985 - \frac{15309}{T} \right) \right] \right\} \quad (8)$$

both evaluated in  $\text{m}^2/\text{s}$ , where  $T$  is the temperature in K and  $y_C^\gamma$   
 is the site fraction of carbon in austenite, which is related to the  
 molar fraction of carbon  $x_C^\gamma$  by the relation  $y_C^\gamma = x_C^\gamma / (1 - x_C^\gamma)$ .

The FDM algorithm was applied in independent grids cor-  
 responding to the different phases considered in the problem.  
 In order to couple all grids without violating the conservation  
 laws, the boundary value problem at the interfaces was evalu-  
 ated by means of the following equation:

$$- D_C^\alpha \frac{dc^\alpha}{dz} \Big|_{int} + v (c_{int}^\gamma - c_{int}^\alpha) = - D_C^\gamma \frac{dc^\gamma}{dz} \Big|_{int} \quad (9)$$

At the immobile martensite-austenite interface, evaluation  
 of equation 9 for  $v = 0$  implies that the flux of carbon must  
 be equal in both phases. In turn, for the migrating bainitic fer-  
 rite/austenite interface the boundary condition becomes a Ste-  
 fan problem considering the interface velocity determined – in  
 the mixed-mode model – by equation 3. Neumann boundary  
 condition representing zero flux of carbon was applied to the  
 extremities of the calculation domain in order to keep the do-  
 main as a closed system.

### 3. Simulation conditions

Two Fe-C alloys with different initial carbon compositions  
 were chosen for the calculations, a low carbon steel Fe-0.25 wt %C  
 and a high carbon alloy Fe-0.8 wt %C. Following Andrews equa-  
 tion [31], martensite start temperatures ( $M_s$ ) were estimated to  
 be 433 and 201 °C, respectively. Alloying elements commonly  
 used in Q&P steels (e.g., Mn and Si) were neglected, as addi-  
 tional variables would be introduced. Moreover, it was found

by previous thermodynamical calculations that such elements do not considerably affect the compositions of equilibrium and constrained carbon equilibrium in a way the results could lead to misleading interpretations.

Different initial martensite-austenite morphologies were employed for each alloy, reflecting the effect of the carbon in the morphology of martensite. For the Fe-0.25 wt %C alloy a film morphology was assumed, as previously used by Santofimia et al. [6], consisting of martensite and austenite films with 0.20  $\mu\text{m}$  and 0.06  $\mu\text{m}$  of thickness (23 vol % of austenite), as represented in Figure 1a. Nucleation of a single bainitic ferrite

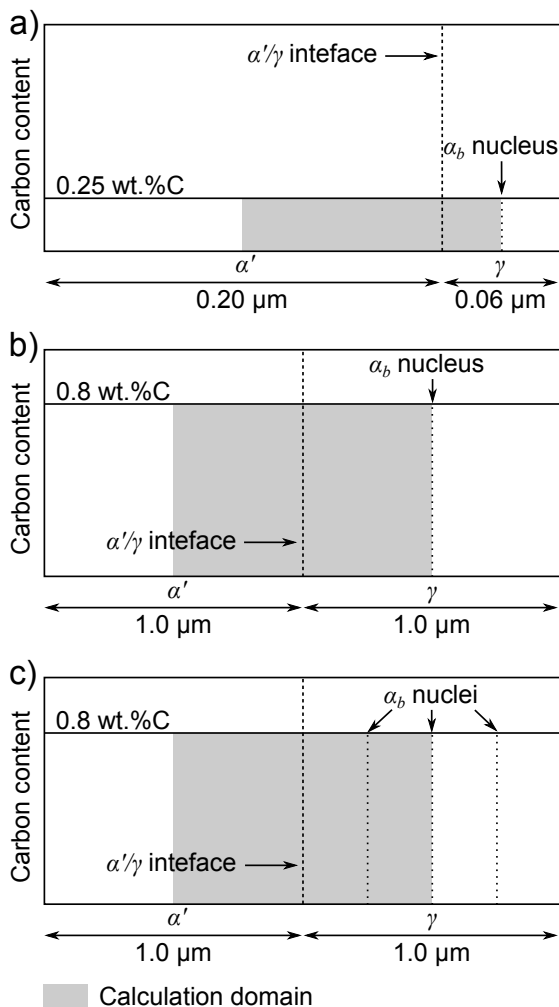


Figure 1: Schematic illustration of the morphologies considered in the simulations for a) Fe-0.25 wt %C alloy, b) Fe-0.8 wt % alloy with one initial nucleus of  $\alpha_b$ , and c) Fe-0.8 wt % alloys with three nuclei of  $\alpha_b$ .

plate is assumed to occur in the middle of the austenite film at  $t = 0$ , when the partitioning step begins. All simulations were carried out assuming the partitioning temperature of 350  $^{\circ}\text{C}$ , as previously considered by Santofimia and coworkers.

Martensite in high carbon alloys presents plate morphology considerably coarser than in low carbon steels and, since the Ms temperature is lower, a greater fraction of austenite is expected at the same quenching temperature. Thus, for the Fe-0.8 wt %C alloy a microstructure consisting of a martensite plate 1.0  $\mu\text{m}$

thick adjacent to a block of austenite 1.0  $\mu\text{m}$  thick (50 vol % of austenite) has been considered. Such dimensions are consistent with martensite morphologies reported in works on Q&P applied to alloys with similar carbon compositions [8, 12]. Regarding the bainite reaction, two scenarios have been considered for this alloy. In the first, a single bainitic ferrite plate is nucleated at instant  $t = 0$  in the middle of the austenite block (Figure 1b). In the second scenario, three bainitic ferrite plates are nucleated equally spaced in the austenite block at  $t = 0$  (Figure 1c). Despite the fact that nucleation usually occurs heterogeneously at defects, the homogeneous nucleation assumption is necessary in the 1D simulations, since the calculation domain does not provide an extra dimension into which the particle could grow.

In order to build a gradual understanding of the studied phenomena, the martensite-austenite carbon partitioning and the bainite reaction were first approached separately for the low carbon alloy. In addition, as most of the works in the literature assume the simplification of constant carbon diffusivity, the effect of adopting this simplification was tested by comparing the cases where constant  $D_C^{\gamma}$  and composition dependent  $D_C^{\gamma}$  are assumed. The carbon partitioning was simulated using the same geometry employed in the coupled model. Simulations of the bainitic ferrite growth were conducted considering an austenite film with the same dimensions as the untransformed austenite in the coupled model.

The chemical potentials of carbon and iron at the partitioning temperature were determined by thermodynamical calculations using the TCFE8 database with the Thermo-Calc $^{\circ}$  software. Additionally, in order to account for the discrepancy between the experimental and computationally determined thermodynamical limits for the bainite reaction, the chemical potentials of the bainitic ferrite were modified by considering the WBs theory. Following the extrapolation proposed by Hillert, the extra energy for the bainite reaction at 350  $^{\circ}\text{C}$  is 1965 J/mol. This energy was summed up to the chemical potentials of bainitic ferrite, leading to a carbon content in austenite of approximately 1.75 wt % at the metastable equilibrium, as is visualized in Figure 2.

## 4. Results and discussion

### 4.1. Effect of carbon diffusivity on kinetics of carbon partitioning

Figure 3a shows the evolution of carbon profiles during the partitioning process simulated assuming a constant value of  $D_C^{\gamma}$  equals to  $1.72 \times 10^{-17} \text{ m}^2/\text{s}$ ; Figure 3b shows the carbon profiles obtained assuming composition dependence of  $D_C^{\gamma}$ . In both cases the carbon content of austenite at interface is very high for short partitioning times and gradually decreases as the carbon partitioning proceeds. Similar results have been previously reported in the literature [5, 6]. It is remarkable that when  $D_C^{\gamma}$  is assumed constant, the carbon composition at the interface reaches a peak value of 6.99 wt %, which is higher than the fraction of carbon in cementite. On the other hand,

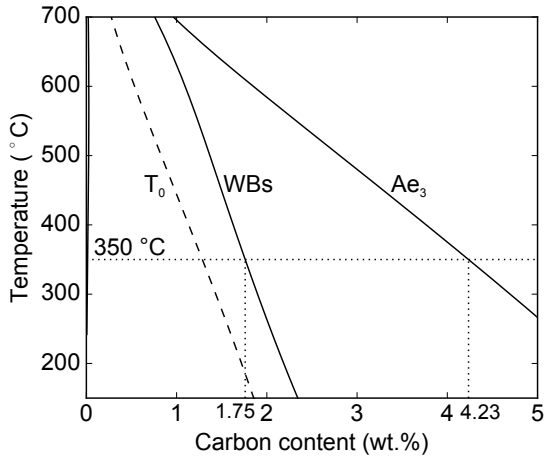


Figure 2: Fe-C phase diagram showing lines proposed to be the critical limit for growth of bainitic ferrite ( $Ae_3$ , WBs, and  $T_0$ ).

when the composition dependence on the diffusivity is considered the maximum composition is 3.11 wt %. Furthermore, carbon in martensite at the interface quickly decreases to values near zero when the effect of carbon concentration on the diffusivity is considered ( $< 0.01$  wt % after 0.01 s). It is also noticed that the gradient of carbon in austenite is different for each condition. The carbon profiles in martensite are relatively flat when  $D_C^\gamma$  is constant. In turn, a steeper gradient is observed in martensite at the interface when the composition dependence of  $D_C^\gamma$  is considered.

These observations can be explained by how the carbon diffusivity affects the mass balance of carbon in the system. It can be proven [14] that, as long as soft impingement has not occurred (i.e., for short times), the following relation must be fulfilled in order to satisfy the mass conservation at the interface:

$$\frac{D_{C\ int}^{\alpha'}}{D_{C\ int}^\gamma} = \left( \frac{c_{int}^\gamma - c^0}{c^0 - c_{int}^\alpha} \right)^2 \quad (10)$$

where  $c^0$  is the initial carbon content, and  $c_{int}^p$  and  $D_{C\ int}^p$  are the fraction of carbon and diffusion coefficient of carbon in the phase  $p$  at the interface. Evaluation of the diffusion coefficient of austenite (eq. 7) implies that an increase of 1 wt % in the carbon increases the carbon diffusivity by about one order of magnitude. Thus, the high concentration of carbon at the interface leads to a local increase of the carbon diffusivity, decreasing the  $\frac{D_{C\ int}^{\alpha'}}{D_{C\ int}^\gamma}$  ratio. Therefore, when the composition dependence of  $D_C^\gamma$  is considered,  $c_{int}^\gamma$  and  $c_{int}^\alpha$  must be lower in order to equation 10 be satisfied. For times longer than 0.1 s soft impingement occurs in martensite and interfacial compositions decrease, deviating from the values predicted by equation 10. It is worth mentioning that the values of  $c_{int}^\gamma$  and  $c_{int}^\alpha$  are restrained by the local equilibrium of carbon and, therefore, cannot be freely changed.

The kinetics of carbon partitioning can be quantitatively visualized by means of the evolution of the average carbon content of martensite and austenite with time (Figure 3c). For con-

stant  $D_C^\gamma$  the martensite is completely decarburized after about 2 s, whereas the same state is reached after only 0.1 s when the composition dependence of  $D_C^\gamma$  is considered. In both cases, once the martensite plate is completely decarburized the composition of austenite reaches the value predicted by the CCE model (1.12 wt %). The different kinetics are explained on basis of which process controls the carbon partitioning. For composition dependent  $D_C^\gamma$  the carbon partitioning is controlled by carbon diffusion in martensite due to the rapid decrease of carbon in martensite at the interface for short times. Conversely, for constant  $D_C^\gamma$  the process is controlled by diffusion in austenite. It is noteworthy that despite the decarburization of martensite being completed after short times ( $< 10$  s), the homogenization of carbon in austenite takes substantially longer. From the carbon profiles, the homogenization of carbon in austenite is reached after 100 s when  $D_C^\gamma$  is assumed constant and 10 s when it varies with composition. This happens because the homogenization depends solely on the carbon diffusion in austenite, which occurs at a slower pace than diffusion in martensite.

The carbon profiles during the growth of a single bainitic ferrite plate are shown in figures 4a (constant  $D_C^\gamma$ ) and 4b ( $D_C^\gamma$  varies with composition). In the mixed-mode model the compositions at the interface gradually evolve from the initial composition to the composition of (metastable) equilibrium. This composition is dictated by the WBs limit, corresponding to a carbon concentration of 1.75 wt %. At the beginning, the system is in a non-equilibrium state where the chemical potential of iron is higher in austenite than in ferrite, leading to a positive chemical driving force for the growth of the ferrite into the austenite. As the growth of bainitic ferrite proceeds, the carbon rejected from ferrite progressively builds up in austenite, the interfacial composition approaching the composition of equilibrium. When the equilibrium is reached the chemical potential of iron is equalized across the interface and, consequently, there is no more chemical driving force to be dissipated and the interface stops. The final transformed fraction and the final position of the interface, determined by the lever rule, are 85 wt % and 0.0045  $\mu\text{m}$ , respectively.

In the carbon profiles the dotted lines represent the carbon content of austenite at the interface plotted as a function the position of the interface. In both cases these lines show inflections as the interfaces advance, representing a decrease of the interface velocity. In Figure 4b the carbon profile at 1.5 s shows that at this stage the diffusion field of carbon ahead of the interface interferes with the diffusion field coming from the other half of the austenite, i.e., soft impingement occurs. Soft impingement leads to a faster accumulation of carbon in the untransformed portion of austenite, therefore leading to a faster decrease of the chemical potential of carbon in austenite and the chemical driving force for the interface migration (eq. 1). Consequently the interface slows down at a higher rate, causing the observed inflections.

The comparison of the evolution of the interface positions with time is shown in Figure 4c. The results are also compared with an analytical solution assuming constant diffusivity in austenite and equilibrium compositions at the interface (dashed line). In the simulated curves the interface moves faster

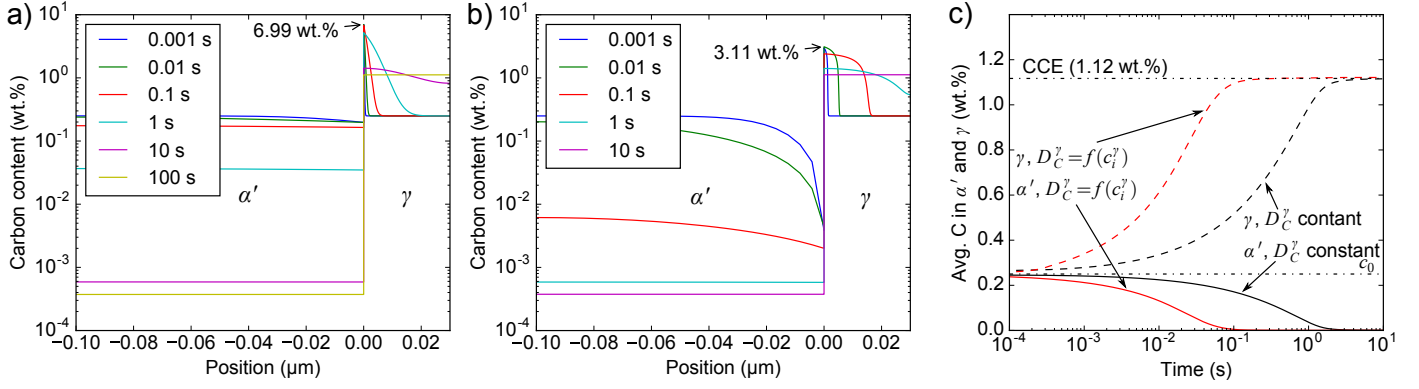


Figure 3: Simulation of  $\alpha'/\gamma$  carbon partitioning. a) Carbon profiles determined assuming  $D_C^\gamma$  constant. b) Carbon profiles obtained assuming the dependence of the carbon content in  $D_C^\gamma$ . c) Comparison of the evolution of the average carbon content in  $\alpha'$  and  $\gamma$  assuming  $D_C^\gamma$  constant (black lines) and varying with the composition ( $D_C^\gamma = f(c_i^\gamma)$ , red lines).

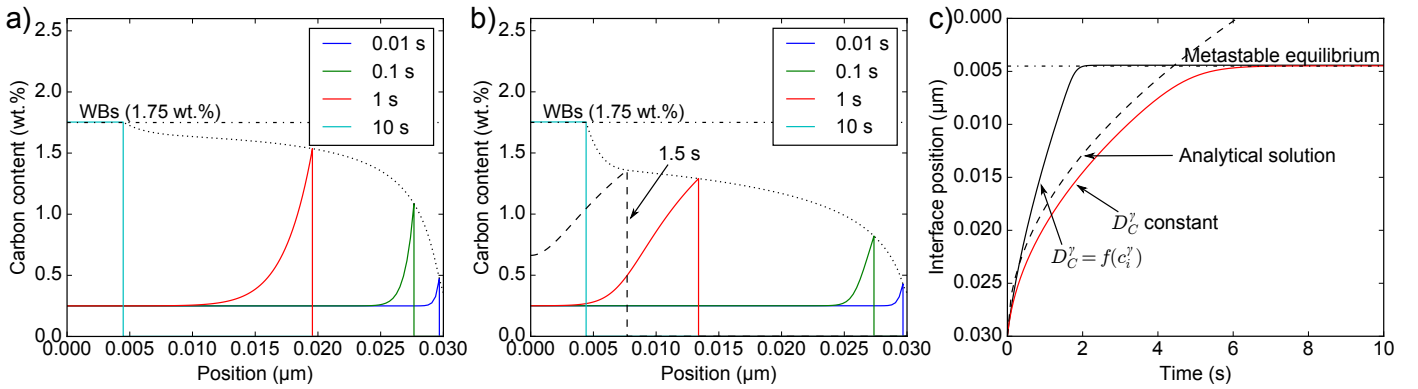


Figure 4: Simulation of growth of single plate of  $\alpha_b$ . a) Carbon profiles determined assuming  $D_C^\gamma$  constant. b) Carbon profiles obtained assuming the dependence of the carbon content in  $D_C^\gamma$ . c) Comparison of the evolution of the  $\alpha_b/\gamma$  interface position.

in the beginning and slows down by soft impingement when the position of equilibrium (0.0045  $\mu\text{m}$ ) is approached. The analytical solution does not account for soft impingement and therefore equilibrium state is never reached in this case. As a consequence of the higher diffusivity in austenite, the kinetics is faster when  $D_C^\gamma$  varies with the composition than when  $D_C^\gamma$  is constant (for both simulated case and analytical solution). However, the growth rate according to the analytical solution is slightly higher than in the simulated constant  $D_C^\gamma$  case, despite the similar assumptions. This difference is observed because the interface migration in the mixed-mode model is limited by its mobility  $M$ , while the analytical solution effectively consists of an extreme case where  $M$  is infinite and the interface velocity depends only on the diffusion of carbon in austenite.

From the above results, it is clear that the composition dependence of diffusivity has an important effect on the kinetics of the phase transformations taking place during the Q&P process. In the next section, the simulations considering the simultaneous occurrence of the bainite reaction and the martensite-austenite carbon partitioning are presented considering this effect.

## 4.2. Coupling martensite-austenite carbon partitioning and bainite reaction

### 4.2.1. Low carbon alloy

Figure 5a shows the carbon profiles obtained with the coupled model for the low carbon alloy (0.25 wt.%C) partitioned at 350  $^\circ\text{C}$ . The vertical lines represent the position of the interfaces at the end of the simulation. As in the case of martensite-austenite carbon partitioning, for short times the carbon profiles in austenite are very sharp close to the martensite-austenite interface and attenuate for longer times. The carbon content of martensite at the interface quickly drops to a value near zero, leading to a process controlled by the carbon diffusion in martensite. A flat carbon profile in austenite, denoting its homogenization, is obtained after 10 s.

The development of the carbon profile during the growth of the bainitic ferrite plate can be analyzed by means of Figure 5b, which shows a detail of the austenite-bainitic ferrite interface. The dotted line represents the austenite carbon content at the interface plotted as function of the position of the interface. An inflection in the dotted line is observed at about 0.3 s, associated with a decrease of the interface velocity due to soft impingement, as discussed before. In this case the diffusion fields that interact are those resulting from the carbon partitioning from the martensite and due to the rejection of carbon during the

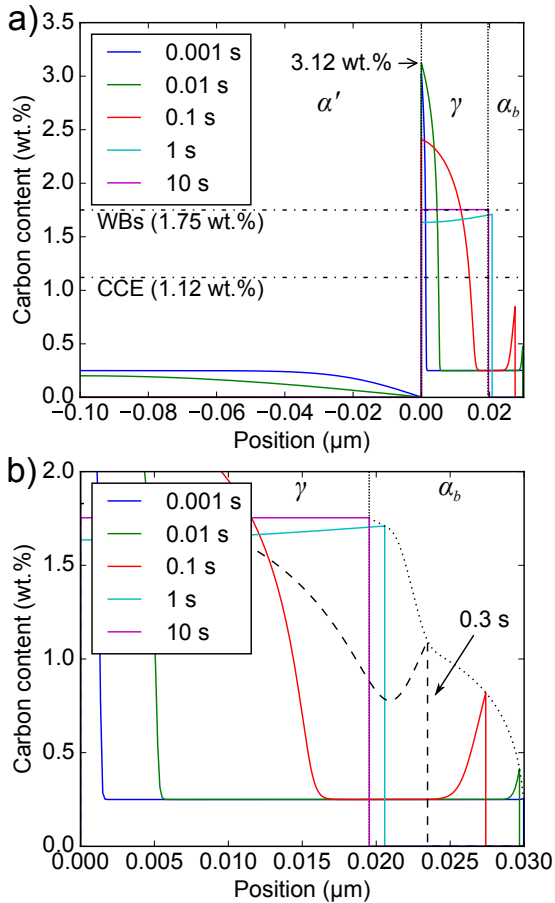


Figure 5: Carbon profiles for the coupled model applied to the low carbon alloy (0.25 wt.%). a) Full carbon profiles. b) Detail of carbon profiles close to the bainitic ferrite plate.

growth of bainite.

Evolution of the average carbon content in martensite and austenite is shown in Figure 6 and compared to the results of the martensite-austenite carbon partitioning case. Evolution of average carbon in martensite (black and red solid lines) shows no different behavior from one case to another. This occurs because the decarburization of martensite is essentially controlled by carbon diffusion in martensite, so that its kinetics depends only on the size and composition of the martensite plate, being virtually insensitive to what occurs in the neighboring austenite. On the other hand, kinetics of carbon enrichment of austenite (dashed lines) shows some important differences. The two curves follow the same trend for very short times ( $< 0.03$  s) but, as the rejection of carbon due to growth of bainitic ferrite takes place, the carbon enrichment of austenite becomes faster in the coupled model, reaching the CCE composition earlier than in the  $\alpha'/\gamma$  case. Moreover, once the austenite-bainitic ferrite interface is free to move, the carbon content of austenite is no longer limited by the CCE composition determined from the initial microstructure and keeps increasing until the equilibrium composition between bainitic ferrite and austenite (i.e., the WBs limit) is reached. In the end, the carbon diffusion achieves the stationary state and the chemical potential of

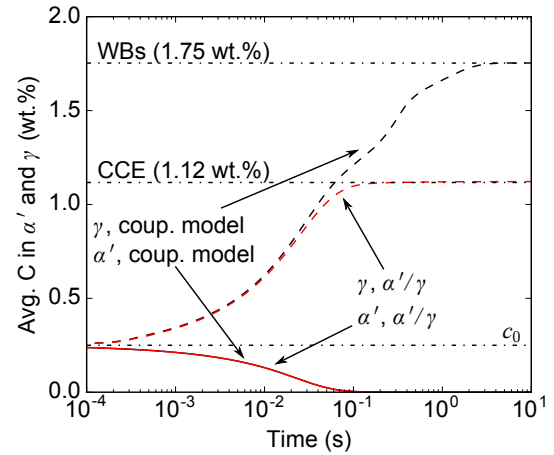


Figure 6: Comparison of the evolution of the average composition of  $\alpha'$  and  $\gamma$  in the coupled model (black lines) and in the  $\alpha'/\gamma$  model (red lines).

carbon becomes homogeneous in the system.

A related point to consider is that the system does not establish a true equilibrium when the carbon profiles achieve the stationary state. Unlike the bainitic ferrite, the chemical potentials of martensite (carbon supersaturated ferrite) were not modified to account for an extra energy and, consequently, the equilibrium compositions for the martensite-austenite pair are given by the extensions of the  $Ae_1$  and  $Ae_3$  lines. Hence, martensite establishes a constrained carbon equilibrium in relation to a microstructure containing the phase fraction of austenite determined by the WBs limit. In the final state, metastable equilibrium between bainitic ferrite and austenite and CCE between martensite and austenite are simultaneously established. Such situation is visualized in the schematic free energies curves shown in Figure 7.

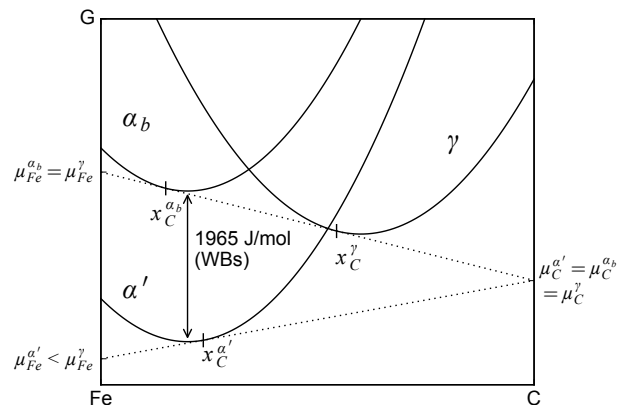


Figure 7: Schematic diagram illustrating the free energies and compositions of the phases in the coupled model when the stationary state is reached.

#### 4.2.2. High carbon alloy

The carbon profiles obtained from the simulations for the high carbon case considering the nucleation of only one bainite plate are shown in Figure 8a. As with all the other discussed

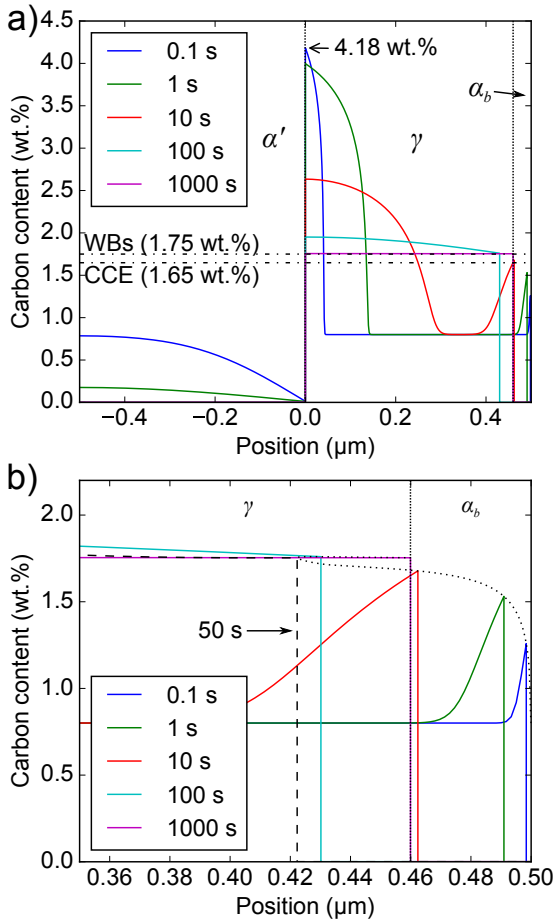


Figure 8: Carbon profiles for the coupled model applied to the high carbon alloy (0.8 wt%) with only one nucleated bainite plate. a) Full carbon profiles. b) Detail of carbon profiles close to the bainitic ferrite plate.

cases, the compositions at the interface experience a rapid rise in austenite and a fast drop in martensite. The higher composition peak at the interface (4.18 wt%) when compared to the low carbon case can be explained on basis of equation 10. When the initial composition  $c^0$  is raised, the right term of eq. 10 is evaluated to a lower value. The equation is balanced when either the ratio  $\frac{D_{\gamma}^{\alpha'}}{D_{\gamma}^{\alpha'}}$  (left term) decreases or when the interfacial compositions increases. Both requisites are simultaneously fulfilled when the interfacial composition of austenite  $c_{int}^{\gamma}$  increases, explaining the result. The carbon partitioning from martensite to austenite takes longer than in the low carbon case, mainly reflecting the coarser simulated microstructure. The martensite plate is completely decarburized after 10 s and the carbon in austenite is homogenized at the WBs composition at about 1000 s.

Carbon profiles in austenite near the bainitic ferrite plate are shown in Figure 8b. At the beginning the interface moves forward consuming austenite, but at 50 s the direction of the interface changes and the plate starts shrinking. Such behavior is more clearly illustrated in Figure 9a, in which the evolution of the interface position and the carbon content in austenite at the interface are exposed. When the interface shifts its direction

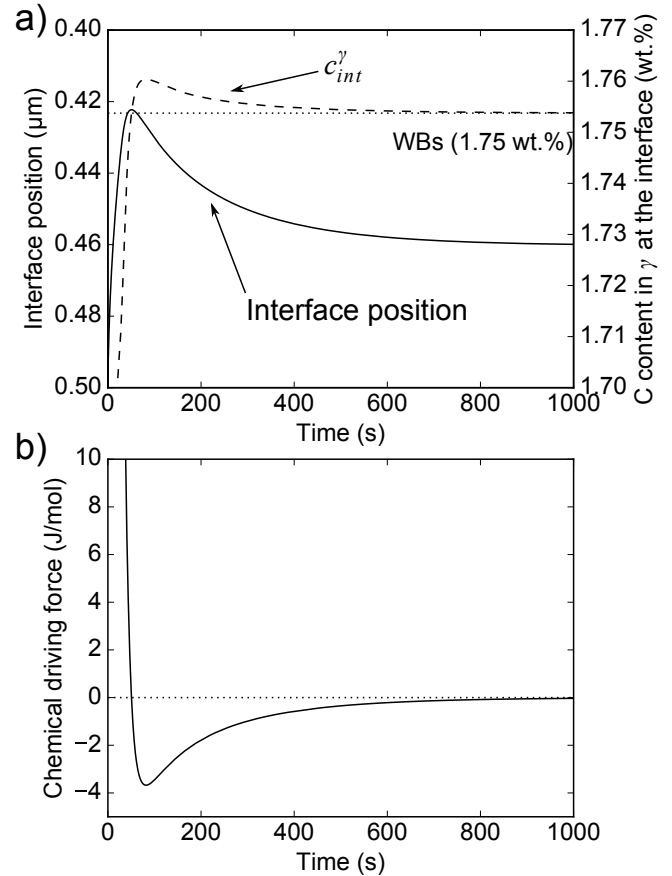


Figure 9: a) Evolution of position of the  $\alpha_b/\gamma$  interface with time (solid line) superimposed with the composition of austenite at the same interface (dashed line). b) Evolution of the chemical driving force available for  $\alpha_b$  growth.

of motion, the interfacial composition of austenite ( $c_{int}^{\gamma}$ ) reaches the WBs composition and continues further increasing due to the carbon partitioned from the martensite. Once the carbon concentration in austenite is higher than the equilibrium value, the chemical potential of iron becomes higher in austenite than in ferrite. This causes the chemical driving force available for bainite growth to become negative (as shown in Figure 9b), which in turn induces the interface moving back towards the bainitic ferrite plate. Additionally, the change of the interface motion causes the development of a negative composition gradient in austenite in order to keep the mass balance preserved. At the moment the interface shifts its motion this gradient is zero, as can be seen in the carbon profile at 50 s (dashed line).

Carbon profiles for the case assuming nucleation of three bainite nuclei in austenite are presented in Figure 10. Because of the symmetry condition at the extremities of the simulated domain, only two (one and a half) bainitic ferrite plates,  $\alpha_{b1}$  and  $\alpha_{b2}$ , are represented in the figure. Regarding the carbon partitioning from martensite, this simulation represents all the previously reported phenomena. However, in contrast to the last case, the present scenario exhibits two austenite regions ( $\gamma_1$  and  $\gamma_2$ ) separated by the bainitic ferrite plates. The three mobile bainitic ferrite-austenite interfaces are named  $i_1$ ,  $i_2$ , and  $i_3$ , as

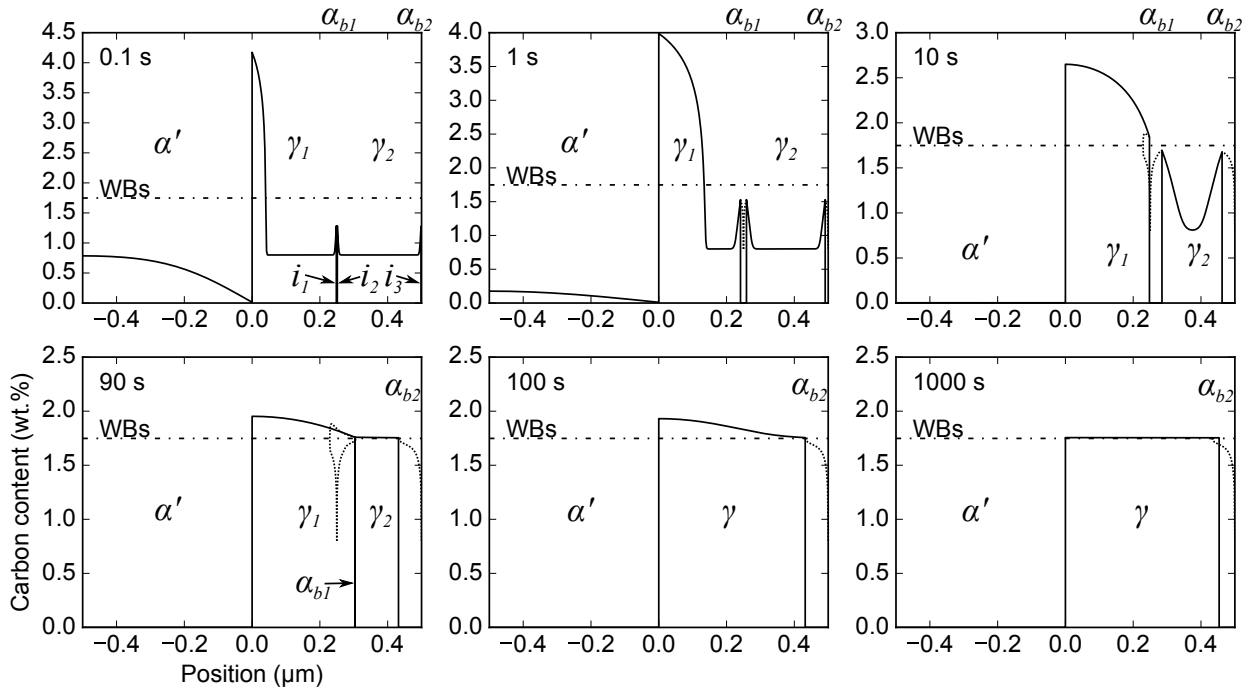


Figure 10: Carbon profiles for the coupled model applied to the high carbon alloy (0.8 wt %) with three nucleated bainite plates.

indicated in the figure.

Due to the smaller dimensions of the austenite blocks, soft impingement occurs after a shorter time than in the case assuming only one bainite plate. The carbon content in the austenite grain closer to the martensite ( $\gamma_1$ ) rapidly increases, surpassing the WBs composition and reversing the movement of the interface  $i_1$  after only 4 s. The other austenite grain ( $\gamma_2$ ) experiences soft impingement of the diffusion fields originated from the carbon rejected during the growth of the bainite plates. After 50 s the carbon in  $\gamma_2$  is completely homogenized at the WBs composition, which is accompanied by the full stop of interfaces  $i_2$  and  $i_3$ . However, interface  $i_1$  keeps moving backwards as long as the equilibrium state in  $\gamma_1$  is not achieved. As this state is not achieved before  $\alpha_{b1}$  is completely dissolved, at about 90 s, a single austenite block,  $\gamma$ , is formed. This situation is illustrated by the carbon profile at the imminence of dissolution of the plate, shown in Figure 10. Afterwards, the excess of carbon in austenite causes the reversal of the movement of the interface  $i_3$ , establishing a situation similar to the one-bainite plate scenario. The remaining bainitic ferrite plate keeps dissolving until the carbon in austenite is homogenized at the WBs composition, which happens at about 1000 s.

In this work the martensite/austenite interface migration has been neglected in order to avoid too many variables being simultaneously evaluated in the model, in spite of such mobility being experimentally observed in some alloys [4, 32]. Indeed, carbon partitioning results in a difference of chemical potentials of iron (and substitutional elements) across the interface, leading to a driving force for martensite/austenite interface migration [33]. However, whether interface migration will occur or not depends on various factors, such as composition, orien-

tation relationship, martensite morphology [32], and pinning of interface dislocations by segregation [34, 35]. The influence of the martensite/austenite interface migration on carbon partitioning was modeled by Santofimia et al. considering different interface mobilities [5, 6]. In accordance to the results of the present model, Santofimia's model showed that kinetics of decarburization of martensite is very fast and it is little affected by interface migration. On the other hand, evolution of carbon profiles in austenite and interface position is very sensitive to interface mobility. In the case of a incoherent interface, Santofimia showed that carbon partitioning induces interface migration towards austenite for short times and then back to martensite for longer times. For the case of a semicoherent interface, carbon profiles for short times are similar to those obtained in the immobile interface case, while for longer times the interface moves towards the martensite plate. In both cases equilibrium between the bcc and fcc phases is approached for longer partitioning times, such as in the present model.

The effect of mobility of the austenite/bainitic ferrite interface on carbon partitioning can be interpreted in a similar way to Santofimia's conclusions for martensite/austenite interface migration. In the case of adopting a mobility value infinitely large, the plate thickening of bainite would be controlled by carbon diffusion. Since the martensite/austenite carbon partitioning is governed by the carbon diffusion in martensite – much faster than carbon diffusion in austenite – the kinetics of martensite decarburization would be little changed from the prediction of the current model. On the other hand, a lower value of the interface mobility would imply a longer time necessary for the homogenization of carbon in austenite.

The effect of varying the quenching temperature is also worth

discussing. As shown in the simulations, dissolution of bainitic ferrite occurs by excess of carbon in austenite at the vicinity of the  $\alpha_b/\gamma$  interface. A higher fraction of martensite is produced at a lower quenching temperature. In this situation, the amount of carbon available to partition to austenite will be larger, enhancing the dissolution process of bainitic ferrite. There will be a critical quenching temperature where any bainitic ferrite precipitate will be completely dissolved at the end of the partitioning step.

In summary, results show that carbon partitioning from martensite to austenite significantly affects the kinetics of the bainite reaction. Partial or total dissolution of bainitic ferrite plates occurs due to accumulation of carbon coming from martensite to the adjacent austenite. The kinetics of these phenomena can be partly explained by the 1D approach used in the current work. When the problem is approached in two or three dimensions, carbon is able to diffuse through other routes not represented in the 1D case. Consequently, carbon is more prone to be trapped in isolated regions in 1D simulations than in 2D/3D simulations. This behavior explains the development of a more heterogeneous distribution of carbon along austenite grains in 2D/3D simulations, as pointed out by Takahama et al. [15].

Moreover, the kinetics of carbon partitioning is little affected by simultaneous occurrence of the bainite reaction. The thermodynamical conditions in the martensite-austenite interface imply that carbon in martensite at the interface decreases to zero at very short times, staying at a nearly constant value until the end of the partitioning step. Consequently, the rate of carbon partitioning becomes controlled by carbon diffusion in martensite. The decarburization time will be essentially affected only by the dimensions of the martensite plate and the initial carbon content. On the other hand, presence of carbides might play a substantial role in defining the kinetics of carbon partitioning. Once the carbides are formed in martensite, carbon partitioning will be only possible if this is accompanied by dissolution of carbides [7], which is presumably a process much slower than diffusion of carbon in martensite. The effect of carbides precipitation on the kinetics of carbon partitioning is currently being pursued and will be presented in future work.

## 5. Conclusions

The redistribution of carbon during the partitioning step of the Q&P process has been assessed by means of a modeling approach that considers the simultaneous occurrence of partitioning of carbon between martensite and austenite and formation of bainitic ferrite. Two alloy compositions (low and high carbon) and different configurations for the bainite nuclei were considered in the simulations. The main conclusions obtained from this work are summarized as follows:

1. Composition dependence of the diffusion coefficient of carbon in austenite substantially affects the results and should not be disregarded in the simulations. When  $D_C^\gamma$  is assumed constant the martensite-austenite carbon partitioning is governed by diffusion in austenite and it is

about 10 times slower than when  $D_C^\gamma$  varies with composition.

2. When the bainite reaction is suppressed the system reaches the constrained carbon equilibrium (CCE) at the endpoint. When bainite reaction is considered the system establishes a metastable equilibrium between bainitic ferrite and austenite and the CCE between martensite and austenite.
3. The interfacial composition of martensite decreases to values near zero for short partitioning times, causing the kinetics of martensite-austenite carbon partitioning to be controlled by diffusion of carbon in martensite. The rate of decarburization of the martensite plates is not affected by the simultaneous occurrence of the bainite reaction. However, rate of carbon-enrichment of austenite is sped up when formation of bainitic ferrite is considered.
4. The kinetics of the bainite reaction is strongly influenced by martensite-austenite carbon partitioning. The carbon partitioned from martensite accumulates in austenite and slows down the growth of bainitic ferrite, eventually causing the reversal of the movement of the interface. If the bainitic ferrite plate is nucleated close enough to the martensite plate it can be completely dissolved by the described phenomena.

## Acknowledgments

Arthur Nishikawa acknowledges financial support by Capes (grant 7409/2015-00 PDSE). Hélio Goldenstein acknowledges partial funding by CNPq.

## References

- [1] J. Speer, D. K. Matlock, B. C. De Cooman, J. G. Schroth, Carbon partitioning into austenite after martensite transformation, *Acta Materialia* 51 (9) (2003) 2611–2622. doi:10.1016/S1359-6454(03)00059-4.
- [2] A. J. Clarke, J. G. Speer, M. K. Miller, R. Hackenberg, D. V. Edmonds, D. K. Matlock, F. C. Rizzo, K. Clarke, E. De Moor, Carbon partitioning to austenite from martensite or bainite during the quench and partition (Q&P) process: A critical assessment, *Acta Materialia* 56 (1) (2008) 16–22. doi:10.1016/j.actamat.2007.08.051.
- [3] E. De Moor, S. Lacroix, A. J. Clarke, J. Penning, J. G. Speer, Effect of Retained Austenite Stabilized via Quench and Partitioning on the Strain Hardening of Martensitic Steels, *Metallurgical and Materials Transactions A* 39 (11) (2008) 2586–2595. doi:10.1007/s11661-008-9609-z.
- [4] D. De Knijf, M. J. Santofimia, H. Shi, V. Bliznuk, C. Föjer, R. Petrov, W. Xu, In situ austenite-martensite interface mobility study during annealing, *Acta Materialia* 90 (2015) 161–168. doi:10.1016/j.actamat.2015.02.040.
- [5] M. J. Santofimia, L. Zhao, J. Sietsma, Model for the interaction between interface migration and carbon diffusion during annealing of martensite-austenite microstructures in steels, *Scripta Materialia* 59 (2) (2008) 159–162. doi:10.1016/j.scriptamat.2008.02.045.
- [6] M. J. Santofimia, J. G. Speer, A. J. Clarke, L. Zhao, J. Sietsma, Influence of interface mobility on the evolution of austenite-martensite grain assemblies during annealing, *Acta Materialia* 57 (15) (2009) 4548–4557. doi:10.1016/j.actamat.2009.06.024.
- [7] F. HajjAkbar, J. Sietsma, G. Miyamoto, T. Furuhashi, M. J. Santofimia, Interaction of carbon partitioning, carbide precipitation and bainite formation during the Q&P process in a low C steel, *Acta Materialia* 104 (2016) 72–83. doi:10.1016/j.actamat.2015.11.032.

- [8] Y. Toji, G. Miyamoto, D. Raabe, Carbon partitioning during quench-790  
ing and partitioning heat treatment accompanied by carbide precipitation,  
Acta Materialia 86 (2015) 137–147. doi:10.1016/j.actamat.2014.  
11.049.
- [9] J. G. Speer, D. V. Edmonds, F. C. Rizzo, D. K. Matlock, Partition-  
ing of carbon from supersaturated plates of ferrite, with application to 795  
steel processing and fundamentals of the bainite transformation, Current  
Opinion in Solid State and Materials Science 8 (3-4) (2004) 219–237.  
doi:10.1016/j.cossms.2004.09.003.
- [10] H. Y. Li, X. W. Lu, X. C. Wu, Y. A. Min, X. J. Jin, Bainitic transforma-  
tion during the two-step quenching and partitioning process in a medium 800  
carbon steel containing silicon, Materials Science and Engineering: A  
527 (23) (2010) 6255–6259. doi:10.1016/j.msea.2010.06.045.
- [11] M. J. Santofimia, L. Zhao, R. Petrov, C. Kwakernaak, W. G. Sloof, J. Sietsma,  
Microstructural development during the quenching and partition-  
ing process in a newly designed low-carbon steel, Acta Materialia 59 (15) 805  
(2011) 6059–6068. doi:10.1016/j.actamat.2011.06.014.
- [12] A. J. S. T. da Silva, H. Goldenstein, W. L. Guesser, M. F. de Campos,  
Quenching and partitioning heat treatment in ductile cast irons, Materi-  
als Research 17 (5) (2014) 1115–1123. doi:10.1590/1516-1439.  
220713.
- [13] S. Mujahid, H. Bhadeshia, Partitioning of carbon from supersaturated 810  
ferrite plates, Acta Metallurgica et Materialia 40 (2) (1992) 389–396.  
doi:10.1016/0956-7151(92)90313-4.
- [14] M. Hillert, L. Höglund, J. Ågren, Escape of carbon from ferrite plates in  
austenite, Acta metallurgica et materialia 41 (7) (1993) 1951–1957. 815
- [15] Y. Takahama, M. J. Santofimia, M. G. Mecozzi, L. Zhao, J. Sietsma,  
Phase field simulation of the carbon redistribution during the quenching  
and partitioning process in a low-carbon steel, Acta Materialia 60 (6-7)  
(2012) 2916–2926. doi:10.1016/j.actamat.2012.01.055.
- [16] M. G. Mecozzi, J. Eiken, M. J. Santofimia, J. Sietsma, Phase field mod-  
elling of microstructural evolution during the quenching and partition-  
ing treatment in low-alloy steels, Computational Materials Science 112  
(2016) 245–256. doi:10.1016/j.commatsci.2015.10.048.
- [17] R. F. Hehemann, K. R. Kinsman, H. I. Aaronson, A Debate on the Bainite  
Reaction, Metallurgical Transactions 3 (May) (1972) 1077–1094. doi:  
10.1007/BF02642439.
- [18] L. C. D. Fielding, The Bainite Controversy, Materials Science and  
Technology 29 (4) (2013) 383–399. doi:10.1179/1743284712Y.  
0000000157.
- [19] H. I. Aaronson, On the problem of the definitions and the mechanism of  
the bainite reaction, in: Symposium on the "Mechanism of Phase Trans-  
formations in Crystalline Solids", 1968, pp. 270–281.
- [20] M. Hillert, Diffusion in growth of bainite, Metallurgical and Materials  
Transactions A 25 (9) (1994) 1957–1966. doi:10.1007/BF02649044.
- [21] A. Borgenstam, M. Hillert, J. Ågren, Metallographic evidence of carbon  
diffusion in the growth of bainite, Acta Materialia 57 (11) (2009) 3242–  
3252. doi:10.1016/j.actamat.2009.03.026.
- [22] M. Hillert, L. Höglund, J. Ågren, Role of carbon and alloying elements in  
the formation of bainitic ferrite, Metallurgical and Materials Transactions  
A 35 (12) (2004) 3693–3700. doi:10.1007/s11661-004-0275-5.
- [23] M. Gouné, F. Danoix, J. Ågren, Y. Bréchet, C. R. Hutchinson, M. Militzer,  
G. Purdy, S. van der Zwaag, H. Zurob, Overview of the current issues  
in austenite to ferrite transformation and the role of migrating interfaces  
therein for low alloyed steels, Materials Science and Engineering: R: Re-  
ports 92 (March 2016) (2015) 1–38. doi:10.1016/j.mser.2015.03.  
001.
- [24] H. Chen, K. Zhu, L. Zhao, S. Van Der Zwaag, Analysis of transformation  
stasis during the isothermal bainitic ferrite formation in Fe-C-Mn and Fe-  
C-Mn-Si alloys, Acta Materialia 61 (14) (2013) 5458–5468. doi:10.  
1016/j.actamat.2013.05.034.
- [25] Z. Yang, W. Xu, Z. Yang, C. Zhang, S. Van Der Zwaag, A 2D analysis of  
the competition between the equiaxed ferritic and the bainitic morphology  
based on a Gibbs Energy Balance approach, Acta Materialia 105 (2016)  
317–327. doi:10.1016/j.actamat.2015.12.040.
- [26] Y. Xia, G. Miyamoto, Z. G. Yang, C. Zhang, T. Furuhashi, Direct mea-  
surement of carbon enrichment in the incomplete bainite transforma-  
tion in Mo added low carbon steels, Acta Materialia 91 (2015) 10–18.  
doi:10.1016/j.actamat.2015.03.021.
- [27] E. Gamsjäger, M. Militzer, F. Fazeli, J. Svoboda, F. Fischer, Interface  
mobility in case of the austenite-to-ferrite phase transformation, Compu-  
tational Materials Science 37 (1-2) (2006) 94–100. doi:10.1016/j.  
commatsci.2005.12.011.
- [28] H. Chen, S. Van Der Zwaag, A general mixed-mode model for the  
austenite-to-ferrite transformation kinetics in Fe-C-M alloys, Acta Ma-  
terialia 72 (2014) 1–12. doi:10.1016/j.actamat.2014.03.034.
- [29] J. Ågren, Diffusion in phases with several components and sublattices,  
Journal of Physics and Chemistry of Solids 43 (5) (1982) 421–430. doi:  
10.1016/0022-3697(82)90152-4.
- [30] J. Ågren, A revised expression for the diffusivity of carbon in binary Fe-  
C austenite, Scripta Metallurgica 20 (11) (1986) 1507–1510. doi:10.  
1016/0036-9748(86)90384-4.
- [31] K. W. Andrews, Empirical formulae for calculation of some transforma-  
tion temperatures, Iron and Steel Institute Journal 203 (7) (1965) 721–  
727.
- [32] G. A. Thomas, J. G. Speer, Interface migration during partitioning of  
Q&P steel, Materials Science and Technology 30 (9) (2014) 998–1007.  
doi:10.1179/1743284714Y.0000000546.
- [33] J. G. Speer, R. E. Hackenberg, B. C. Decooman, D. K. Matlock, Influence  
of interface migration during annealing of martensite/austenite mixtures,  
Philosophical Magazine Letters 87 (6) (2007) 379–382. doi:10.1080/  
09500830701194173.
- [34] A. Grajcar, R. Kuziak, W. Zalecki, Third generation of AHSS with  
increased fraction of retained austenite for the automotive industry,  
Archives of Civil and Mechanical Engineering 12 (3) (2012) 334–341.  
doi:10.1016/j.acme.2012.06.011.
- [35] M. Kuzmina, D. Ponge, D. Raabe, Grain boundary segregation engi-  
neering and austenite reversion turn embrittlement into toughness: Ex-  
ample of a 9wt.medium Mn steel, Acta Materialia 86 (2015) 182–192.  
doi:10.1016/j.actamat.2014.12.021.